Journal of Directed Energy, **3**, Winter 2009, 257–275

Measurements of Improved ElectricOIL Performance, Gain, and Laser Power

J. W. Zimmerman*
University of Illinois at Urbana–Champaign, Urbana, Illinois 61801

G. F. Benavides
University of Illinois at Urbana–Champaign, Urbana, Illinois 61801, and CU Aerospace, Champaign, Illinois 61820

B. S. Woodard
University of Illinois at Urbana–Champaign, Urbana, Illinois 61801

D. L. Carroll, A. D. Palla, and J. T. Verdeyen
CU Aerospace, Champaign, Illinois 61820

and

W. C. Solomon
University of Illinois at Urbana–Champaign, Urbana, Illinois 61801

Ongoing experiments have led to continued improvements in the electric oxygen–iodine laser (ElectricOIL) system that significantly increased the performance, gain, and laser power output. Experimental investigations utilize radio-frequency discharges in O_2/He/NO mixtures in the pressure range of 30–60 torr. The goal of these investigations was maximization of both the yield and flow rate (power flux) of $O_2(a^1\Delta)$ in order to produce favorable conditions for subsequent gain and lasing in our ElectricOIL system. Numerous measurements of $O_2(a^1\Delta)$, oxygen atoms and discharge excited states are made to characterize the discharge. A gain of 0.22% cm^{-1} was measured with a corresponding outcoupled power of 28 W. Modeling with the BLAZE-IV code is in good agreement with data and helps to guide our understanding of this complex hybrid laser system.

KEYWORDS: ElectricOIL, Oxygen–iodine laser, Singlet oxygen

Received August 26, 2009; revision received December 2, 2009.
*Corresponding author; e-mail: joseph.w.zimmerman@gmail.com.

Nomenclature

g	gain, proportional to [I*]–0.5 [I]
g_{th}	threshold gain required for laser power extraction
K_{eq}	equilibrium constant of pumping reaction
L_g	gain length
$[O_2]_{inp}$	input density of oxygen adjusted for temperature at measurement location
r	mirror reflectivity
T_g	temperature determined from gain profile
t	mirror transmissivity
Y_{OT}	$O_2(a)$ yield required for optical transparency, [I*] = 0.5 [I]
ΔP	pressure drop across heat exchanger
ΔT	temperature drop across heat exchanger

1. Introduction

The first demonstration of the electric oxygen–iodine laser (often referred to as ElectricOIL, EOIL, or DOIL)[6] was enabled through an understanding of the importance of oxygen atoms in the kinetics of the discharge and postdischarge regions. Oxygen atoms play a positive role in that they rapidly dissociate the I_2 molecule[1] but also play a negative role in that they quench the upper laser level[2] and also directly quench the singlet oxygen metastable $O_2(a^1\Delta)$ [denoted hereafter as $O_2(a)$] through a three-body process.[3] By controlling the atomic oxygen levels through the addition of small molar fractions of NO or NO_2, it is possible to enhance the performance of the system in terms of the $O_2(a)$, the gain, and the laser power.[5,6] Ionin et al.[9] provide a comprehensive topical review of discharge production of $O_2(a)$ and ElectricOIL studies. Over the past 5 years of research and development, continual improvements in $O_2(a)$ production, gain, and lasing power have been obtained. In this paper we discuss recent discharge and configuration improvements that have led to more than two orders of magnitude enhancement in gain and laser power since our initial demonstration of 0.002% cm^{-1} and 0.16 W, respectively, to 0.22% cm^{-1} and 28 W (with a 5-cm gain length cavity).

2. Transverse Discharge Experiments

Recent experimental results have shown that, at moderate pressures of 40–100 torr, the discharge production of $O_2(a)$ is increased by reducing the diameter of the discharge tube.[14,16] A quartz tube with an outer diameter (OD) of 19 mm (3/4-in.) provided a substantial improvement over the 50-mm-diameter tube at pressures above 30 torr. All of the results reported here were taken using a parallel plate electrode configuration around a 19-mm tube. BLAZE-IV[10,11] modeling results (not shown for brevity) suggested that this was insufficient time for the $O_2(a)$ to reach an equilibrium for its production. To test this theory, the discharge electrodes were lengthened along the tube. A 10-in. (previous standard length for our experiments), 20-in., and 33-in. set of electrodes was created. The flow residence times in the 10-, 20-, and 33-in. discharges are approximately 1.8, 3.3, and 4.7 ms, respectively. The actual length of the discharge is obviously dependent on the length of the electrodes, but it also depends significantly on the discharge power and pressure. Figure 1 shows the $O_2(a)$ yield and the actual discharge length versus power for

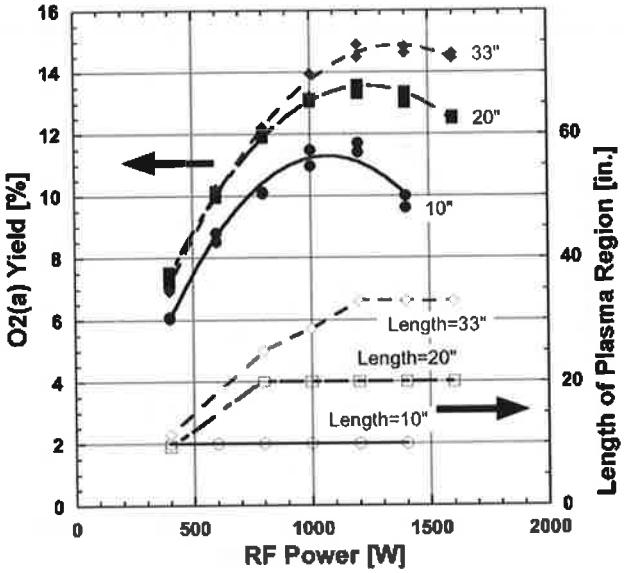

Fig. 1. $O_2(a)$ yield and actual discharge length vs. RF power for three different electrode lengths at 40 torr and flow rates of 10:33:0.2 and O_2:He:NO.

each of the three electrode lengths. The pressure in all the cases shown in Figs. 1–4 is 40 torr, and the flow rates are 10:33:0.2 of O_2:He:NO. At this pressure, the 10-in. discharge fills the electrodes for all the powers shown. The data in these figures were taken at a fixed distance downstream from the exit of each discharge. The yield reaches a higher value with the longer electrodes, although more power is required to reach the peak $O_2(a)$ yield as the electrodes are lengthened. The yield of $O_2(b^1\Sigma)$ [denoted hereafter as $O_2(b)$] is shown in Fig. 2, and the trend is generally the opposite that of $O_2(a)$. The $O_2(b)$ yield decreases substantially from the 10-in. electrode case, whereas the values for the 20- and 33-in. cases are similar. The higher $O_2(b)$ yield in the 33-in. discharge as compared to the 20-in. discharge is unexpected; this phenomenon is still under investigation. The flow temperature derived from the rotational spectrum of the $O_2(b)$ is given in Fig. 3. For a given input radio-frequency (RF) power, the resulting flow temperature depends little on the length of the discharge. This result implies that in order to take advantage of the higher $O_2(a)$ yields provided by the longer discharge at higher powers, the flow will be hotter than in the lower yield case, which is a challenge that can be alleviated with a properly designed postdischarge heat exchanger (Sec. 3). Figure 4 shows the dissociation fraction measured downstream of the discharge, upstream of the heat exchanger. Similar to the temperature, the residence time within the discharge appears to have little impact on the production of oxygen atoms.

Increasing the flow's residence time in the discharge produces more $O_2(a)$ while creating less $O_2(b)$ and approximately the same concentration of oxygen atoms. These results appear to be very encouraging and will be tested in the full laser system in the near future to determine whether we observe enhancements in gain and lasing performance from the increases in $O_2(a)$ yield.

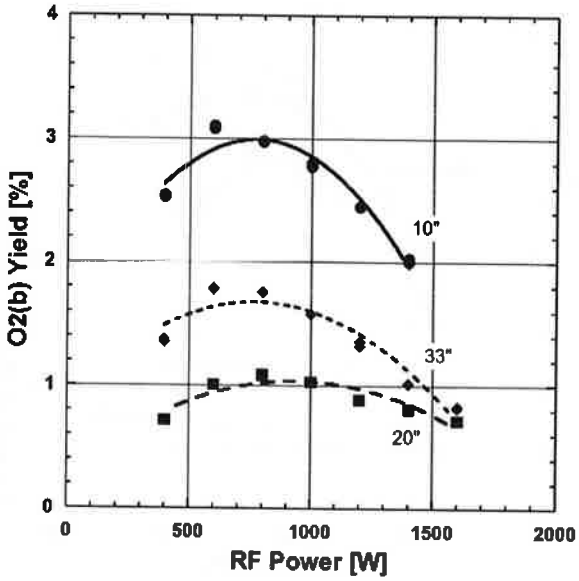

Fig. 2. $O_2(b)$ yield vs. input RF power for three different electrode lengths at 40 torr and flow rates of 10:33:0.2 and O_2:He:NO.

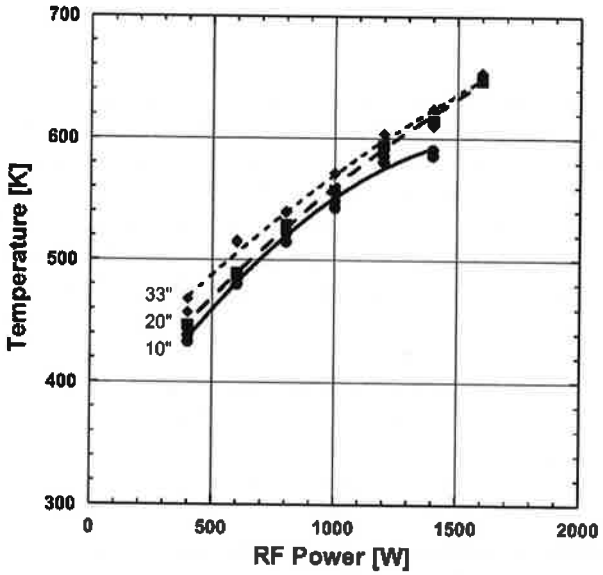

Fig. 3. Flow temperature vs. RF power for three different electrode lengths at 40 torr and flow rates of 10:33:0.2 and O_2:He:NO.

3. Thermal Management

In the ElectricOIL system, the discharge exit flow temperature is typically in the range of 550–650 K; therefore it is important to properly engineer thermal management solutions for the ElectricOIL system. Because the equilibrium of the pumping reaction is temperature

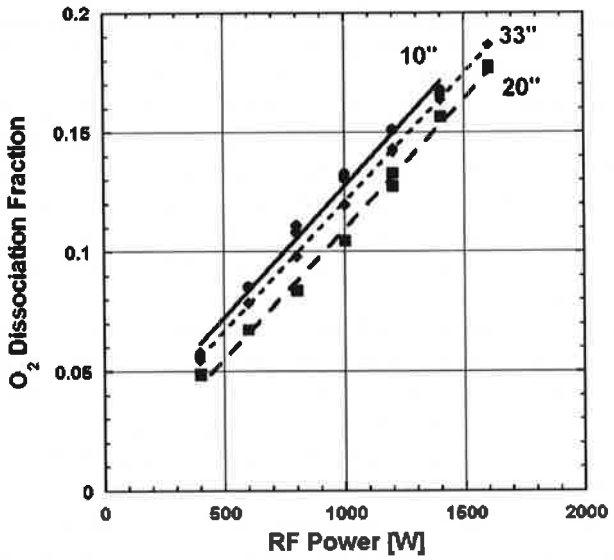

Fig. 4. O_2 dissociation fraction vs. RF power for three different electrode lengths at 40 torr and flow rates of 10:33:0.2 and O_2:He:NO.

dependent [Eqs. (1)–(2)], it is preferable to reduce the temperature to 300 K or less (a temperature comparable to classical COIL) before entering the supersonic nozzle and lasing cavity. Utilizing a supersonic cavity with a Mach 2.4 geometric profile, the resulting flow temperature is generally less than 150 K. A low flow temperature in the resonator region is desirable because of the reduction in the threshold $O_2(a)$ yield for optical transparency:

$$O_2(a) + I \rightleftarrows O_2 + I^*, \tag{1}$$

$$Y_{OT} = \frac{1}{1 + 2K_{eq}} = \frac{1}{1 + 1.5\exp(401.42/T)}. \tag{2}$$

Numerous methods of heat removal have been implemented or are in the process of being tested in our laboratory. Looking at ElectricOIL in a stepwise fashion, the first opportunity for heat removal is prior to the discharge. The gases being fed to the discharge may be precooled to near–liquid oxygen temperatures (~90 K). Because of the heat introduced into the discharge and the warm discharge tube walls, this technique does not result in a huge temperature benefit following the discharge. A discharge exit temperature drop of approximately 20 K was measured experimentally. Because other techniques to cool the discharge gases have proven to be more effective (discussed below), this method has not been used in the ElectricOIL laser beyond a handful of experimental studies.

Next, the discharge itself may be cooled. An effective approach may be to water cool each electrode by installing channels within the electrodes. This proved to be effective in a low-power system used by Rakhimova et al.[13] Hill[8] has reported success cooling his discharge array with nonconductive chilled liquid Fluorinert, reporting a discharge exit temperature in the area of 398 K. An older version of ElectricOIL, which utilized a 2-in.-diameter water-cooled discharge tube and longitudinal electrodes, demonstrated an exit temperature drop of 15–20 K; although this was an encouraging result, it also was not as large a drop

as needed and other postdischarge methods proved to be more effective. However, newer flat-plate rectangular designs may soon permit cooling of the discharge region to be tested with better effectiveness. Currently the discharge is air cooled.

Downstream of the discharge, air cooling of the flow tubes can remove a considerable amount of heat. The helium carrier gas in the flow does an excellent job of conducting heat to the quartz or Pyrex flow tube walls. The thermal conductivity of helium is 0.21 W/m-K compared to 0.04 W/m-K for oxygen. Currently, fans blowing high-flow-rate air are directed on the flow tubes in order to remove heat from the system. During operation, turning these fans on and off has a significant impact on the laser performance, demonstrating their simple yet valuable role.

The engineering solution that has worked best in our experimental setup is a water-cooled or cryogenic heat exchanger downstream of the discharge, the focus of this section. Issues related to a heat exchanger can become complex and require effort to solve. Heat exchangers function by introducing a fluid to a substantially cooler surface with preferentially a very great surface area to maximize heat transfer. In the case of ElectricOIL, increases in surface area can result in increased deactivation of the desired $O_2(a)$ state, thereby reducing lasing performance. From the standpoint of preserving $O_2(a)$, minimizing surface area between the discharge and resonator is ideal. Clearly the goals of maximizing heat removal and minimizing $O_2(a)$ loss conflict in a real apparatus. However, because reducing the flow temperature ultimately reduces the $O_2(a)$ threshold, so long as the usable concentration of $O_2(a)$ above threshold increases faster than the concentration lost due to wall deactivation, significant benefit can be obtained. It is also well known that some wall materials deactivate $O_2(a)$ at a slower rate than other materials; thus investigations into possible wall coatings may also help mitigate the extent to which $O_2(a)$ is deactivated.

Downstream of the heat exchanger, an inert cold gas can be injected into the primary flow prior to the resonator to reduce the flow temperature. This method of temperature reduction has been quite effective in our laboratory experiments and has played an important role in achieving better performance. On the downside, the added gas increases the system pressure, which in turn drops the $O_2(a)$ yield and concentration. Ideally, a highly effective design for a heat exchanger will be found such that the addition of cold gas can be substantially reduced or eliminated.

3.1. Heat exchanger experimental setup

The experimental setup used for the heat exchanger investigation is illustrated in Fig. 5. A flow comprising 20 mmol of oxygen per second, 66 mmol of helium per second, and a small quantity of nitric oxide (~0.25 mmol/s) is premixed and divided between two 3/4-in.-OD quartz tubes. The gas flow in each tube travels between two 10-in.-long thin-plate copper electrodes touching the outside of each quartz tube. The pair of transverse discharges are driven in parallel using a 13.56-MHz ENI OEM-25A RF power supply. The gas temperature at the end of the discharge region, just prior to the heat exchanger, is determined from the $O_2(b)$ rotational spectral emission at 762 nm using an Apogee E47 charge-coupled device (CCD) camera coupled to a Roper Scientific/Acton Research 150-mm monochromator. The detector is repositioned at each of the diagnostic blocks to take additional $O_2(b)$ emission immediately downstream of the heat exchanger and considerably farther downstream of the heat exchanger where the gas has diffused to become more uniform. A Princeton Instruments Optical Multi-channel Analyzer (OMA-V, 1,024-element InGaAs array) with a 0.3-m Acton monochrometer and a 600-g/mm grating blazed at 1.2 μm was used for

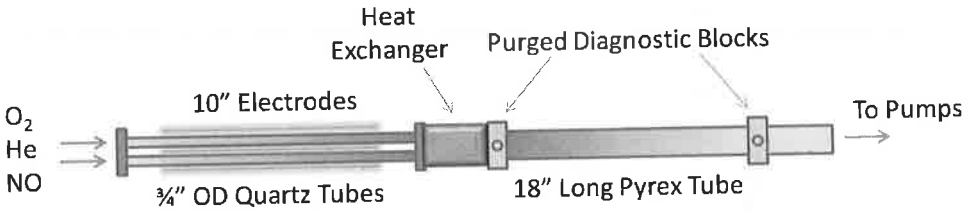

Fig. 5. Experimental setup.

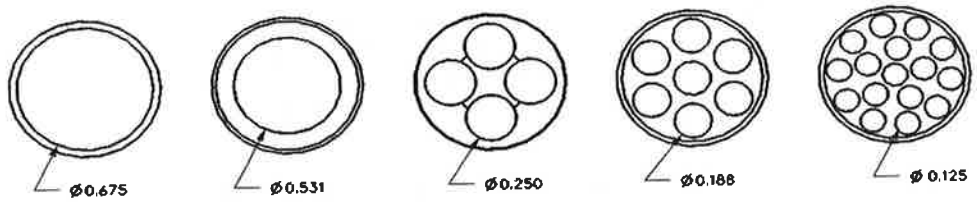

Fig. 6. Circular duct design configurations that were tested.

measurements of $O_2(a)$ at 1,268 nm. Measurements of $O_2(a)$ were made exclusively at the second downstream diagnostic block. The O_2 dissociation fraction was determined using NO_2* emission (air afterglow) at the second diagnostic block. The broadband emission of NO_2* was measured using a Hamamatsu R955 photomultiplier with a narrowband 580-nm filter and a 50-mm-focal-length collection lens; the O atom concentration (and equivalently the O_2 dissociation fraction) was determined from NO_2* using the method described by Piper.[12]

The discharge gaseous output then enters the heat exchanger and passes through some number of small circular ducts (Fig. 6), in this case machined from ¾-in.-OD aluminum rod stock, while 285-K tap water circulates the exterior jacket. The exterior geometry of the heat exchanger was selected based on the discharge geometry to which it interfaced, in this case ¾-in.-OD quartz tubes. The concepts discussed herein can be easily applied to other discharge geometries (or other technologies requiring a heat exchanger). Thus far, five internal geometries have been constructed and tested, as illustrated in Fig. 6.

The gas exits the heat exchanger with a reduced temperature and diffuses into a 2-in.-OD Pyrex tube. Ideally, we would prefer to make measurements of both $O_2(a)$ and $O_2(b)$ at the upstream diagnostic block position to ascertain the performance of each heat exchanger configuration; however, the NO_2* broadband emission at this location and the complex geometry of the diffusing gas make measurements immediately downstream of the heat exchanger highly convoluted. The 18-in.-long Pyrex tube, though, provides sufficient distance for the NO_2* broadband emission to become insignificant compared with the $O_2(a)$ and $O_2(b)$ intensities as well as permitting the gas to fully diffuse to ensure comparable flow uniformity between heat exchanger measurements. Using knowledge of the varying wall temperature on the Pyrex tube and measurement of the flow temperature at the second diagnostic block, the temperatures presented herein have been extrapolated back to the first diagnostic block position. The $O_2(a)$ and O_2 dissociation fraction data (derived from O atom concentration measurements) presented here are collected at the second diagnostic block. No attempt has yet been made to extrapolate the data back to the heat exchanger exit at this time. In other words, although the $O_2(a)$ and O_2 dissociation fraction data are of interest for

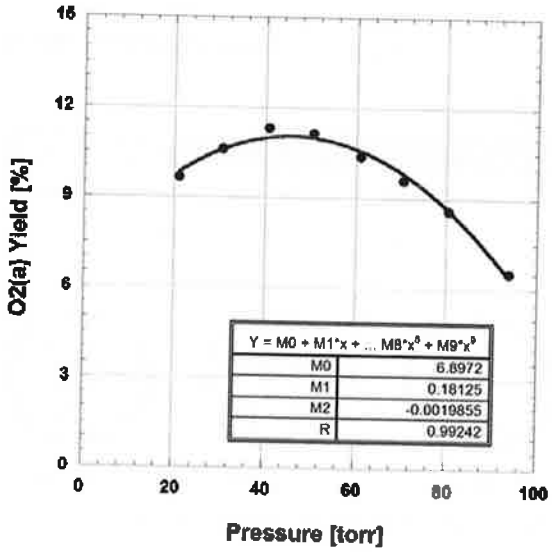

Fig. 7. O_2(a) yield vs. discharge pressure for a 10-in.-long discharge section. Discharge flow conditions are O_2:He:NO = 10:33:0.15 mmol/s, with a discharge power of 800 W.

their absolute magnitudes at the first diagnostic block, the relative differences between heat exchanger configurations can be assessed using data taken at the second diagnostic block.

3.2. Heat exchanger experimental results

Figure 7 shows that the O_2(a) yield as a function of discharge pressure does not vary much in the region of 30–60 torr; this figure illustrates the relationship of O_2(a) production with pressure in a single ¾-in.-OD quartz tube at a fixed RF power of 800 W. This allows us to be fairly confident that for any significant differences in O_2(a) yield downstream of the heat exchanger, the probable cause will be the heat exchanger geometry and/or material, not discharge output.

The geometry of each heat exchanger results in a unique pressure loss ΔP as illustrated in Fig. 8. Not surprisingly, the heat exchanger with the greatest number of and smallest ducts results in the greatest pressure loss, whereas a single thin-walled tube results in the least pressure loss. To ensure comparable data, the pressure in the downstream Pyrex tube was maintained between 42 and 43 torr, whereas the discharge pressure was allowed to vary based on the heat exchanger. This provides the most pertinent information because in conjunction with the lasing cavity, the nozzle throat does in fact maintain the flow pressure downstream of the heat exchanger regardless of heat exchanger configuration (making allowances of course for a small pressure change resulting from the differences in temperature created by the efficiency of each heat exchanger). The variation in discharge temperature resulting from discharge pressure change with each heat exchanger configuration is shown to be small in Fig. 9. The variation in temperatures is essentially within the experimental error of the temperature measurement technique.

Figure 10 illustrates the expected result that an increase in surface area and a decrease in diffusion distance to the wall results in an improvement in temperature reduction.

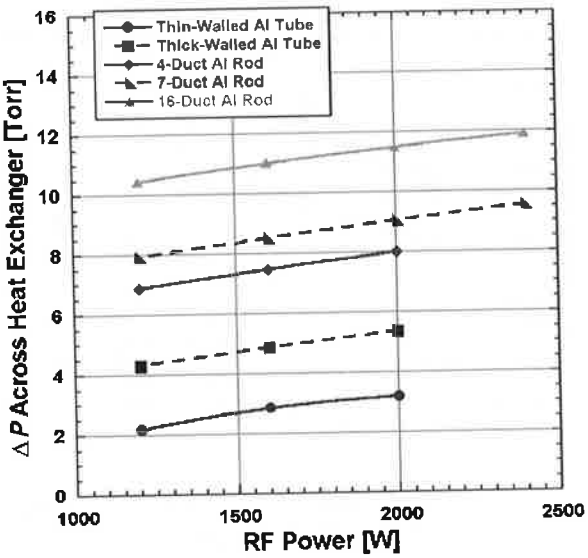

Fig. 8. Pressure drop vs. RF power as a function of heat exchanger configuration.

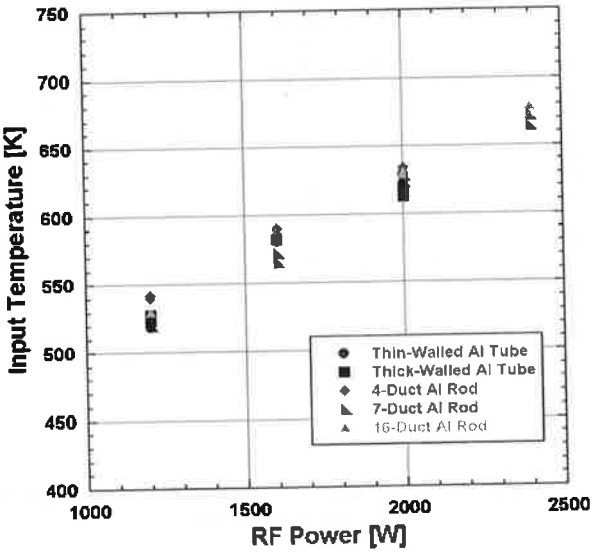

Fig. 9. Heat exchanger input temperature (approximately the same as the discharge exit temperature) vs. RF power.

Alternatively, the change in temperature, rather than the absolute temperature, is plotted in Fig. 11. Interestingly, the 7- and 16-duct layouts provide very similar results. It is likely that a heat transfer limit is being reached due to the increasingly small temperature gradient between the heat exchanger exit temperature and the coolant temperature and as a result of a relatively long conduction distance from the central duct walls to the exterior wall interfacing with the circulating coolant. A recommended next step is to reduce

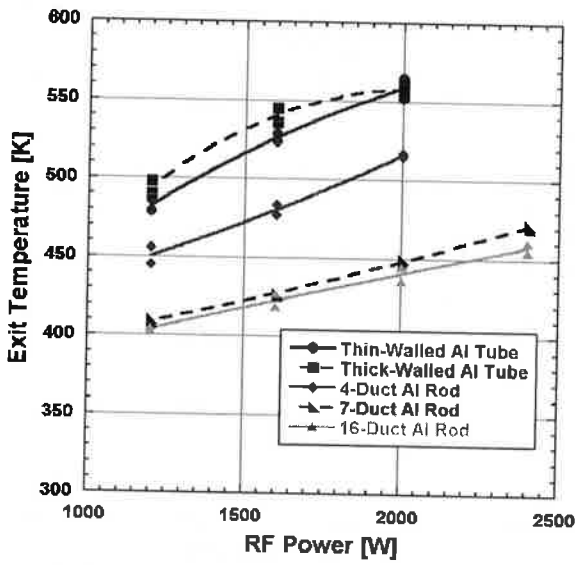

Fig. 10. Heat exchanger exit temperature vs. RF power.

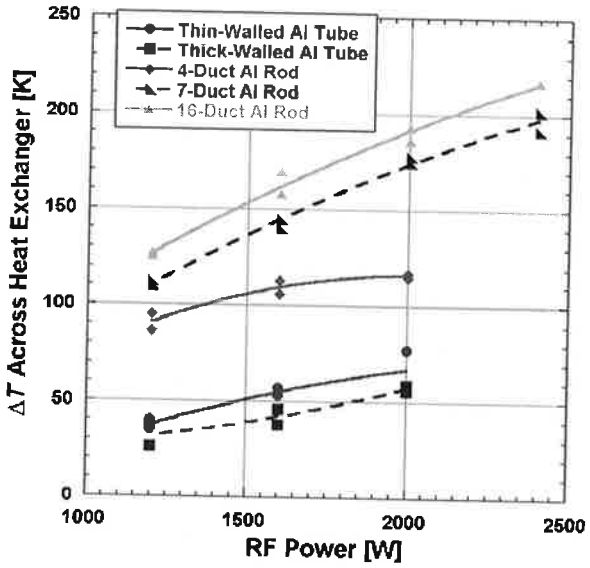

Fig. 11. Change in temperature (ΔT) across heat exchanger vs. RF power.

the coolant temperature to cryogenic levels to see how low of a flow temperature can be reached. Further decreasing the flow temperature in the heat exchanger will increase the residence time of the gas in the heat exchanger (due to a decrease in flow velocity as the flow temperature drops), but it will probably result in minimal change to the $O_2(a)$ loss. In other words, decreasing the coolant temperature provides considerable room for improvement without risking a significant increase in $O_2(a)$ deactivation. Theoretical modeling currently in progress will help narrow the range of possible layouts to test in the search for a near optimal configuration.

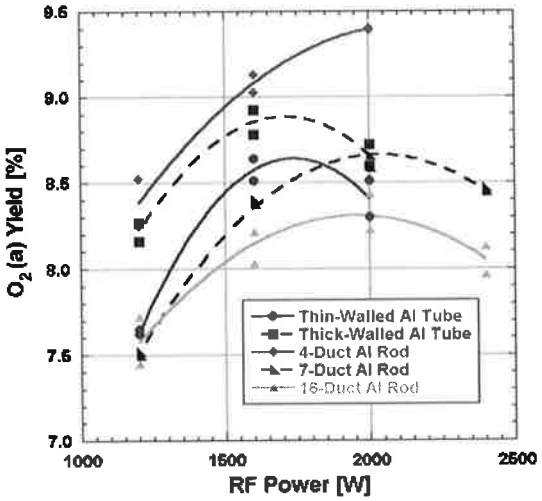

Fig. 12. O_2(a) yield vs. RF power.

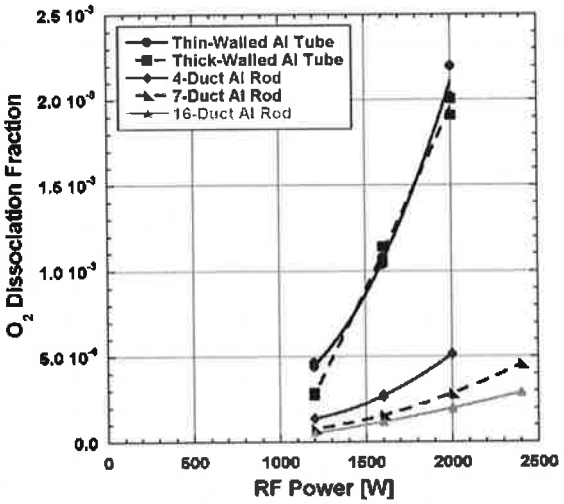

Fig. 13. O_2 dissociation fraction vs. RF power.

Figure 12 demonstrates that no drastic variation occurs in the O_2(a) yield as a result of increasing the temperature reduction efficiency of the heat exchanger. At worst, the yield drops from around 9.4% to 8.2% (Fig. 12 at 2,000 W), but the addition of the heat exchanger drops the gas temperature by around 190 K (Fig. 11 at 2,000 W). In subsequent gain and laser experiments (Sec. 4), we always found that this trade-off has proven to strongly favor using the heat exchangers with the 7- and 16-duct layouts; in other words, dropping the gas temperature significantly outweighed a 1% loss in O_2(a) yield. Figure 13 shows that the heat exchanger is useful not only for removing heat from the flow but also for reducing the O_2 dissociation fraction. Because the heat exchanger increases the pressure upstream

of the heat exchanger as well as the pressure throughout its own ducts, determining what mechanism is ultimately responsible for the greater part of the reduction in O atoms will require additional modeling and testing. These additional data will address the question of how much of the reduction in O atoms is strictly the result of recombination on the heat exchanger walls versus how much is due to increased recombination in the flow as pressure increases.

Returning to the $O_2(a)$ yield presented in Fig. 12, it makes sense that the $O_2(a)$ yield increases slightly at the second diagnostic block when changing from the thin-walled tube to the four-duct layout. The four-duct layout provides a significant reduction in O-atom concentration in the flow, which in turn means that less $O_2(a)$ decay as a result of collisions with O atoms is occurring in the flow between the two diagnostic blocks. In short, more of the $O_2(a)$ leaving the heat exchanger is surviving to reach the second diagnostic block than would occur with the thin-walled tube, which has an exit flow with considerably more O atoms. Going from the 4-duct layout to the 7- or 16-duct layout results in only moderately fewer O atoms in the flow, whereas the geometry of those heat exchangers results in greater deactivation of $O_2(a)$. Thus, we begin to see how design of the heat exchanger for an ElectricOIL system is governed by numerous variables, including variables as easily overlooked as the residence time from the heat exchanger exit to the resonator.

4. Gain and Laser Enhancement Experiments and Modeling

As we acquire more understanding of the complex ElectricOIL system, including the species output from the discharge and the resulting downstream kinetics, we have implemented a logical progression of knowledge into evolving generations of the ElectricOIL system to increase the gain and laser power output levels. Previous results have been presented from third- and fourth-generation laser cavities, "Cav3"[3] and "Cav4."[15] Zimmerman et al.[15] investigated the use of two parallel primary discharges at higher total flow rates and pressure. The $O_2(^1\Delta)$ was produced by two parallel capacitive 13.56-MHz electric discharges sustained in an O_2–He–NO gas mixture, and I^* was then pumped using energy transferred from $O_2(^1\Delta)$; the electrode gaps in the primary discharges were transverse to the flow direction, and the discharges were matched in parallel from a single power supply. Both of the plasma zones filled the transverse gap and were approximately 1.6-cm diameter and 25 cm long (the OD of each of these discharge tubes was 1.9 cm). In prior Cav3 experiments, a single 4.9-cm-diameter plasma zone was utilized (discharge tube with OD of 5.1 cm). The change to smaller diameter discharge tubes was motivated by a detailed series of work summarized in Braginsky et al.,[4] in which they demonstrated that smaller diameter tubes had substantially increased discharge stability at higher pressure while maintaining significant $O_2(^1\Delta)$ yields. More information on the performance of the transverse electric discharge sustained in an O_2–He–NO gas mixture used in those two-tube experiments, as well as those presented herein, can be found in Woodard et al.[14] and Zimmerman et al.[16] The primary advantages to this discharge arrangement were (i) the ability to take advantage of the improved performance of the smaller discharge tubes; (ii) higher total flow rates of the gases, thereby increasing the number densities of the excited species; and (iii) distribution of the higher total flow through a higher number of small tubes, allowing discharge pressure of 40–55 torr rather than pressures >75 torr.

The newest results were obtained with a fifth-generation laser cavity, "Cav5" (Fig. 14), that includes four 3/4-in. discharges feeding into a single 5-cm-gain-length laser cavity, as

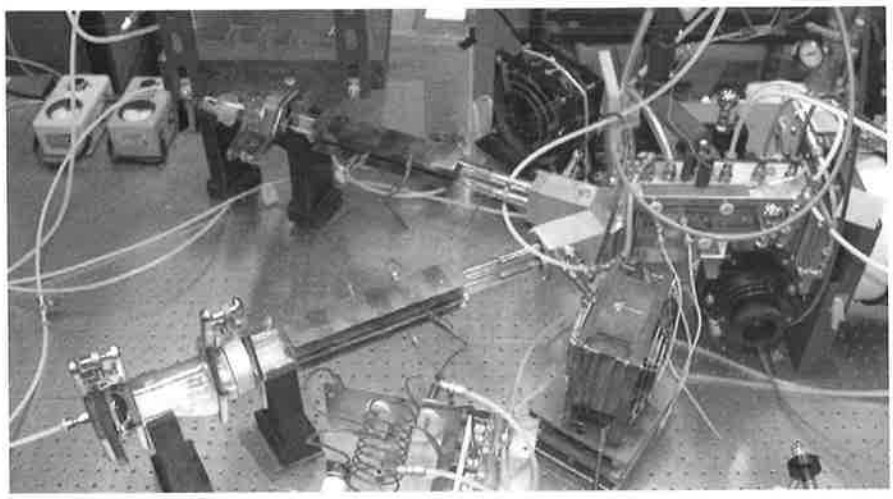

Fig. 14. Photograph of the fifth-generation Cav5 laser cavity experimental apparatus driven by four ¾-in. discharge tubes.

well as compact heat exchangers (Sec. 3) that reduce both the flow temperature and the concentration of oxygen atoms. The Cav5 experiments to date were run without the addition of a secondary RF discharge[3] to predissociate the molecular iodine.

The flow conditions for these gain and laser power experiments with the quad primary discharges are 30.0 mmol of O_2 per second, which is diluted with 100.0 mmol of He per second and $\approx$ 0.20 mmol of NO per second. A secondary stream of $\approx$0.30 mmol of I_2 per second with 55.0 mmol of secondary He diluent per second was injected 27.8 cm downstream from the exit of the primary discharge. A tertiary flow of 240 mmol of cold N_2 gas ($\approx$83 K) per second was injected farther downstream to lower the temperature. The pressures in the discharge section, in the subsonic section downstream of the heat exchanger (with the seven-hole configuration; Fig. 6), and in the supersonic diagnostic cavity were 53.0, 44.3, and 4.7 torr, respectively. Measurements near the exit of the discharge from the $O_2(^1\Delta)$ and $O_2(b^1\Sigma)$ spectra indicated an $O_2(^1\Delta)$ yield of $\approx$11% and a gas temperature of $\approx$570 K for these flow conditions at 650 W of RF power in each of the four discharges (a total of 2,600 W).

Gain was measured for the above flow conditions at a total of 2,600 W of primary RF discharge power. Figure 15 shows the gain at line center, which peaks at 0.22% cm^{-1} with the quad 1.9-cm-diameter primary discharges. For comparison, the best gain previously observed in our system was 0.17% cm^{-1}, using dual 1.9-cm-diameter primary discharges. The line shape indicates a temperature of $\approx$110 K.

Modeling simulations were performed for this case with the BLAZE-IV code.[10,11] BLAZE-IV is an end-to-end discharge through laser cavity model that includes electrodynamics for the discharge section and quasi-one-dimensional fluid equations with multistream mixing terms. Using the baseline mixing parameters established for the older Cav3 hardware, and simply making changes to the geometry and flow/discharge conditions that are appropriate for this Cav5 case, good agreement is found with the gain measurement (Fig. 16), as well as temperature and yield measurements (Fig. 17).

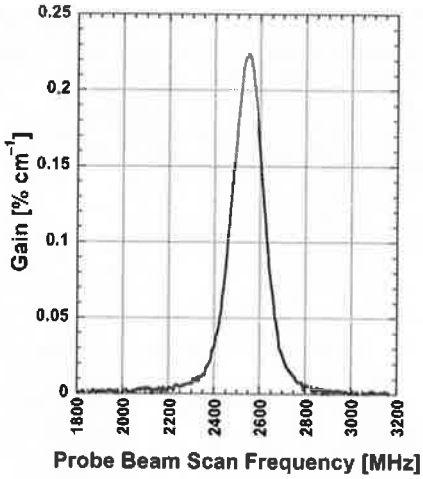

Fig. 15. Gain line shape in the supersonic cavity as a function of probe beam scan frequency with quad 1.9-cm-diameter discharges operating at 53 torr (4.7 torr in supersonic cavity).

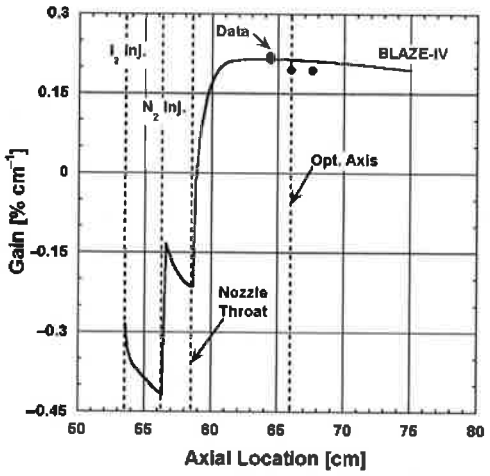

Fig. 16. BLAZE-IV modeling predictions of Cav5 gain from the I_2 injection location through the nozzle and into the supersonic laser cavity region.

The laser resonator was subsequently installed around the 5-cm-gain-length supersonic cavity. Several different mirror combinations were used having different values of threshold gain [$g_{\text{th}} = -\ln(r_1 r_2)/2L_g$] (Table 1 and Fig. 18). For the above 53-torr flow conditions, a total laser output power of 28.1 W was obtained, a 128% improvement in laser power relative to the 12.3-W result from Ref. 15. The beam shape was rectangular with rounded corners and had a length of ≈4.4 cm in the flow direction and a height of ≈2.5 cm (the same dimensions as the clear aperture of the mirror mounts in the flow direction and the height of the nozzle at the center of the beam in the vertical direction). Note that it is possible to make estimates of the laser cavity yield (not shown for brevity) based on these power data, knowledge of the flow rates, and equations found in Hager et al.[7]; these estimates are in

Table 1. Mirror combination sets used in test of ElectricOIL Cav5 quad-discharge tube configuration.

Set	Mirror 1	Mirror 2	r_1	r_2	$r_1 r_2$	g_{th} (cm^{-1})	Power output (W)
1	0702-2	0801-1	0.999950	0.999293	0.999243	7.573×10^{-5}	26.5
2	0801-1	0803-1	0.999293	0.998837	0.998131	1.870×10^{-4}	28.1
3	0702-2	0802-1	0.999950	0.989620	0.989571	1.048×10^{-3}	22.3
4	0706-3	0802-1	0.999889	0.989620	0.989510	1.055×10^{-3}	23.2
5	0803-1	0802-1	0.998837	0.989620	0.988469	1.160×10^{-3}	19.7

For simplicity, the listed values of reflectivity r are based solely on transmission t measurements and are herein assumed to be $r = 1 - t$.

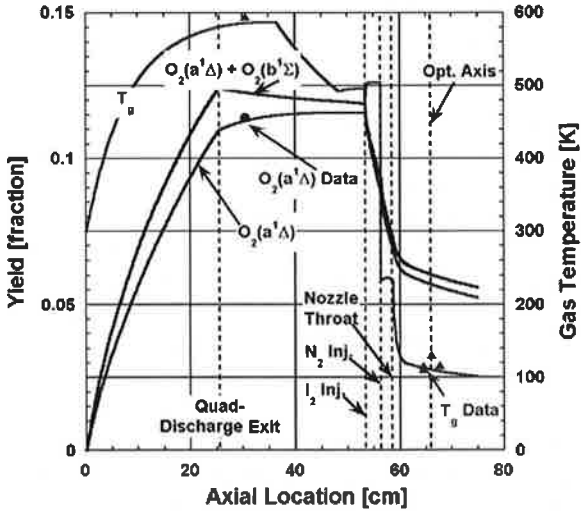

Fig. 17. BLAZE-IV modeling predictions of Cav5 yield and gas temperature from the start of the discharge section through the nozzle and into the supersonic laser cavity region.

reasonable agreement with the BLAZE-IV predictions of approximately 7% yield in the laser cavity region (Fig. 17).

5. Concluding Remarks

Over the past five years of research and development, continual improvements in gain and lasing power have been obtained. The gain has risen from the initial demonstration of 0.002% cm^{-1} by more than two orders of magnitude to 0.22% cm^{-1}, and similarly the outcoupled laser power has risen from 0.16 to 28 W (with a 5-cm-gain-length cavity). We are obtaining significant energy coupling into the desired O_2(a) state (11%–18% for cases discussed in this work), but significant improvements in understanding the role of components of plasma-generated "active oxygen" still need to be made in regard to laser

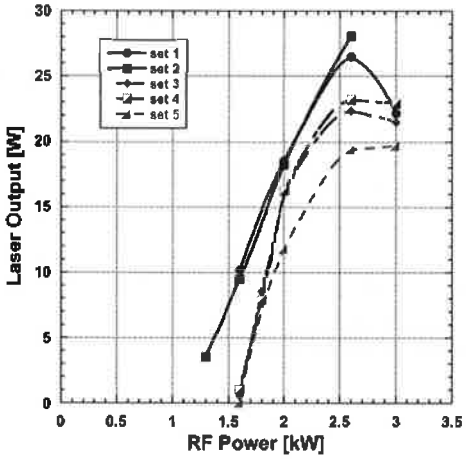

Fig. 18. ElectricOIL Cav5 laser power output (total outcoupled from both mirrors) as a function of the mirror set listed in Table 1.

extraction of this energy. Although O atoms permit rapid dissociation of the I_2 molecule, they appear to be a major problem for energy extraction (as they also act as a quencher), and alternate I_2 dissociation schemes need be investigated.

Geometry is a critical parameter for the production of high $O_2(a)$ yields from transverse RF discharges at moderate pressures (40–60 torr). The discharge that effectively makes $O_2(a)$ at 20 torr does not fill the electrode volume as the pressure increases, and this effect leads to decreased yield. By shortening the gap between the electrodes and lengthening the discharge region, the discharge fills the volume at higher pressures and more effectively creates $O_2(a)$ at those pressures. We have found significant improvements (30% rise) in yield by going from a discharge length of 10 in. to 33 in. Future work will exploit this effect along with other geometry enhancements to create a discharge capable of producing high yields with high oxygen flow rates to produce a flow with high $O_2(a)$ power. The improvement of temperature reduction techniques has been critical toward ElectricOIL's performance enhancements. The postdischarge tube heat exchanger study and experiments proved to be effective in reducing the discharge flow temperature, and additional reductions are planned.

The implementation of a combination of multiple smaller diameter discharge tubes plus an efficient postdischarge tube heat exchanger has permitted us to expand the flow conditions of the ElectricOIL device to higher pressures and flow rates. The use of longer discharge regions with a small discharge gap is showing promising results and will be implemented in future gain/laser testing. A continued expansion of the operating envelope to higher flow conditions, pressures, and gain length of the laser cavity, plus further integration of other performance-enhancing components, are expected to provide increases to the gain and laser power.

6. Acknowledgments

This work was supported by DARPA prime contract HR0011-07-C-0054 on a subcontract from Physical Sciences Inc. (PSI). Additionally, J. Zimmerman was supported by the Directed Energy Professional Society (DEPS) Scholarship Program. The authors gratefully

acknowledge the contributions of W. T. Rawlins, S. J. Davis, and S. Lee (PSI) and M. Heaven (Emory University).

References

[1]Atkinson, R., D. L. Baulch, R. A. Cox, R. F. Hampson, Jr., J. A. Kerr, M. J. Rossi, and J. Troe, J. Phys. Chem. Ref. Data **26**, 550 (1997).

[2]Azyazov, V. N., I. Antonov, S. Ruffner, and M. C. Heaven, SPIE **6101**, 61011Y (2006).

[3]Benavides, G. F., J. W. Zimmerman, B. S. Woodard, D. L. Carroll, J. T. Verdeyen, T. H. Field, A. D. Palla, and W. C. Solomon, Appl. Phys. Lett. **92**, 041116 (2008).

[4]Braginsky, O. V., A. S. Kovalev, D. V. Lopaev, O. V. Proshina, T. V. Rakhimova, A. T. Rakhimov, and A. N. Vasilieva, J. Phys. D: Appl. Phys. **40**, 6571 (2007).

[5]Carroll, D. L., J. T. Verdeyen, D. M. King, J. W. Zimmerman, J. K. Laystrom, B. S. Woodard, G. F. Benavides, K. Kittell, and W. C. Solomon, IEEE J. Quant. Elect. **41**(2), 213 (2005).

[6]Carroll, D. L., J. T. Verdeyen, D. M. King, J. W. Zimmerman, J. K. Laystrom, B. S. Woodard, G. F. Benavides, K. Kittell, D. S. Stafford, M. J. Kushner, and W. C. Solomon, Appl. Phys. Lett. **86**, 111104 (2005).

[7]Hager, G. D., C. A. Helms, K. A. Truesdell, D. Plummer, J. Erkkila, and P. Crowell, IEEE J. Quant. Elect. **32**(9), 1525 (1996).

[8]Hill, A. E., Appl. Phys. Lett. **91**, 041116 (2007).

[9]Ionin, A. A., I. V. Kochetov, A. P. Napartovich, and N. N. Yuryshev, J. Phys. D: Appl. Phys. **40**, R25 (2007).

[10]Palla, A. D., D. L. Carroll, J. T. Verdeyen, and W. C. Solomon, J. Appl. Phys. **100**, 023117 (2006).

[11]Palla, A. D., J. W. Zimmerman, B. S. Woodard, D. L. Carroll, J. T. Verdeyen, T. C. Lim, and W. C. Solomon, J. Phys. Chem. A **111**, 6713 (2007).

[12]Piper, L. G., G. E. Caledonia, and J. P. Kennealy, J. Chem. Phys. **75**, 2847 (1981).

[13]Rakhimova, T. V., A. S. Kovalev, A. T. Rakhimov, K. S. Klopovsky, D. V. Lopaev, Y. A. Mankelevich, O. V. Proshina, O. V. Braginsky, and A. N. Vasilieva, "Radio-Frequency Plasma Generation of Singlet ($a^1\Delta_g$) Oxygen in O_2 and O_2:Ar (He) Mixtures," AIAA Paper 2003-4306 (2003).

[14]Woodard, B. S., J. W. Zimmerman, J. T. Verdeyen, D. L. Carroll, T. H. Field, G. F. Benavides, A. D. Palla, and W. C. Solomon, "Improved Production of $O_2(a^1\Delta)$ in Transverse Radio-Frequency discharges," HPLA 2008 Conference, Taos, NM, April 21–24, 2008; also Proc. SPIE **7005**, 70051L (2008).

[15]Zimmerman, J. W., B. S. Woodard, G. F. Benavides, D. L. Carroll, J. T. Verdeyen, A. D. Palla, and W. C. Solomon, Appl. Phys. Lett. **92**, 241115 (2008).

[16]Zimmerman, J. W., B. S. Woodard, J. T. Verdeyen, D. L. Carroll, T. H. Field, and W. C. Solomon, "Improved Production of $O_2(a^1\Delta)$ in Capacitively-Coupled Radio-Frequency Discharges," LASE 2008 Conference, San Jose, CA, January 21–24, 2008; SPIE **6874**, 68740C (2008).

The Authors

Mr. Gabriel F. Benavides received his B.S. degree in aeronautical and astronautical engineering from the University of Illinois at Urbana–Champaign (UIUC) in 2001. He then worked for CU Aerospace as a Staff Engineer. In 2003, he returned to full-time study at UIUC, pursuing an M.S. degree in aerospace engineering. He received his M.S. in 2004 and is presently a Ph.D. candidate in aerospace engineering at UIUC. He currently conducts experimental research and component-level design and system-level design in the areas of chemical lasers and electric propulsion.

Dr. David L. Carroll received his Ph.D., M.S., and B.S. degrees in aeronautical and astronautical engineering from the University of Illinois at Urbana–Champaign (UIUC) in 1992, 1986, and 1985, respectively. He is a founder of CU Aerospace and is its Engineering Director. Other positions he has held through the years include Member of Technical Staff at TRW in Redondo Beach, California, from 1987 to 1988; Postdoctoral Research Associate at UIUC from 1992 to 1995; Research Scientist at UIUC from 1995 to 2000; and Adjunct Lecturer at UIUC in 2001. He has performed in-depth chemical laser system research for more than 20 years including HF and COIL performance and modeling, materials

processing experiments with COIL, and issues related to the commercialization of these devices. He has also performed research on stimulated Brillouin scattering (SBS) beam combination and genetic algorithms.

Mr. Andrew D. Palla received his A.B. degrees in physics and mathematics from the University of Chicago in 2002 and his M.S. degree in aerospace engineering from the University of Illinois at Urbana–Champaign in 2004. He is currently a Senior Physicist and head of the Modeling and Simulation Division at CU Aerospace, where his focus is on the development of multiphysics computational models for the study of laser systems (gas chemical, gas discharge, and solid-state) and other engineering/physics problems of interest.

Dr. Wayne C. Solomon received his Ph.D. in chemistry from the University of Oregon in 1963 and his B.S. in chemistry from the University of Idaho in 1956. He is a Professor Emeritus at the University of Illinois at Urbana–Champaign (UIUC); was a Professor and Head of the Department of Aeronautical and Astronautical Engineering at UIUC from 1988 to 2001; is a founder and President of CU Aerospace in 1998; was Director of Engineering at Bell Aerospace Textron from 1973 to 1988; was a Staff Scientist with the Air Force at Edwards Air Force Base from 1969 to 1973 and 1963 to 1967; and was a Visiting Professor at the Institute fur Physikalische Chemie, Goettingen, from 1967 to 1969. He joined the faculty at the University of Illinois after directing all the high-energy laser activities at Bell Aerospace Textron. His activities include research for several families of high-energy chemical lasers. Several laser systems that were significantly advanced under his leadership included DF–CO_2, HF space laser devices, DF lasers, and COIL devices. Current research includes COIL laser technology with nitrogen diluent and large-scale CFD modeling of COIL devices.

Dr. Joseph T. Verdeyen received a Ph.D. in electrical engineering from the University of Illinois in 1962, an M.S. from Rutgers University in 1958, and the BSEE degree from Rose-Hulman in 1954. He served with the U.S. Army from 1955 to 1957; was Director of the University of Illinois at Urbana–Champaign Gaseous Electronics Laboratory from 1972 to 1974; was Director of the Compound Semiconductor Microelectronics Laboratory and NSF Center for Compound Semiconductor Microelectronics from 1988 to 1989; has been a Professor Emeritus at the University of Illinois since 1994; and consults as a Senior Scientist to CU Aerospace. After undergraduate studies, he worked for Bell Telephone Laboratories at Murray Hill, New Jersey. After completing his graduate studies, he remained at the University of Illinois as a faculty member in Electrical and Computer Engineering. He has been a consultant to Zenith and Lucitron on plasma display technology, General Electric at Nela Park and Applied Physical Laboratories on lighting, Protech, and TEL on RF discharges and plasma processing, and Sandia and Livermore National Laboratories on microwave and RF discharges. His current research interests are lasers (gas, solid state, and semiconductor), optical communications and control, plasma display technology, and gas phase processing of materials.

Mr. Brian S. Woodard received his B.S. in aeronautical and astronautical engineering in 2001 from the University of Illinois at Urbana–Champaign (UIUC). He then worked for the Department of Aeronautical and Astronautical Engineering as a visiting academic professional until the fall of 2002, when he began pursuing his M.S. degree in aerospace engineering at UIUC. He completed his M.S. in 2004 and is currently a Ph.D. candidate in aerospace engineering at UIUC. During his academic and professional careers he has developed and conducted laboratory experiments encompassing all aspects of creating an electrically assisted oxygen–iodine laser.

Mr. Joseph W. Zimmerman received his B.S. (2001) and M.S. (2003) degrees in aeronautical and astronautical engineering from the University of Illinois at Urbana–Champaign (UIUC). His graduate research involved the modeling of gas discharges for use in oxygen-iodine lasers; presently he is performing experimental investigations on a proposed electrically assisted oxygen–iodine laser concept. He has worked as a Staff Engineer for CU Aerospace and is currently a Ph.D. candidate in aerospace engineering at UIUC.